PROCEEDINGS OF THE ROYAL SOCIETY A

Proc. R. Soc. A (2009) **465**, 3517–3530
doi:10.1098/rspa.2009.0307
Published online 26 August 2009

On the collapse of locally isostatic networks

By V. Kapko[1,*], M. M. J. Treacy[1], M. F. Thorpe[1] and S. D. Guest[2]

[1]*Department of Physics and Astronomy, Arizona State University, P.O. Box 871504, Tempe, AZ 85287-1504, USA*
[2]*Department of Engineering, University of Cambridge, Trumpington Street, Cambridge CB2 1PZ, UK*

We examine the flexibility of periodic planar networks built from rigid corner-connected equilateral triangles. Such systems are locally isostatic, since for each triangle the total number of degrees of freedom equals the total number of constraints. These nets are two-dimensional analogues of zeolite frameworks, which are periodic assemblies of corner-sharing tetrahedra. If the corner connections are permitted to rotate, as if pin-jointed, there is always at least one collapse mechanism in two dimensions (and at least three mechanisms in three dimensions). We present a number of examples of such collapse modes for different topologies of triangular net. We show that the number of collapse mechanisms grows with the size of unit cell. The collapsible mechanisms that preserve higher symmetry of the network tend to exhibit the widest range of densities without sterical overlap.

Keywords: flexibility; locally isostatic networks; zeolites

1. Introduction

In this paper, we examine locally isostatic periodic planar networks of corner-sharing equilateral triangles. In these networks, each triangle is connected at the corners to three neighbours, and each corner is shared between two triangles. The triangles are rigid but can freely rotate in the plane, as if pin-jointed at their corners. The networks, being periodic, are infinite in extent, but can be decomposed into finite repeated units, analogous to unit cells in crystals. By locally isostatic, we mean that, for each rigid unit, the number of degrees of freedom equals the number of constraints. For our plane nets, each equilateral triangle has three degrees of freedom (two translations and one rotation) and six constraints (x and y coordinates for each corner). But each corner is shared between two triangles, so the number of constraints per triangle is also three, rendering these nets locally isostatic.

The three-dimensional analogue of these systems, networks of corner-sharing SiO_4 tetrahedra, provides a model of zeolites. These systems are also locally isostatic with six degrees of freedom per tetrahedron and 12 shared constraints. This 'rigid unit mode' model has been intensively studied by M. Dove and

*Author for correspondence (vitaliy.kapko@asu.edu).

Received 9 June 2009
Accepted 31 July 2009

co-workers (Hammonds *et al.* 1997, 1998), who applied it to diffusion and adsorption in zeolites facilitated by flexibility. More recently, Sartbaeva *et al.* (2006), using geometric simulations, have shown that frameworks of real zeolites can be realized at some range of densities called the 'flexibility window'. They argue that the presence of the flexibility window can be used as a criterion for the selection of potential synthetic targets among the millions of hypothetical zeolite frameworks (Treacy *et al.*, 1997, 2004; Earl & Deem 2006).

Networks of corner-sharing triangles or tetrahedra have the same flexibility properties as pin-jointed frames made of rigid bars placed at triangle edges and connected by frictionless joints. These finite pin-jointed structures have been extensively studied. Maxwell (1864) introduced a simple rule: a system having j joints and no kinematic constraints requires at least $3j-6$ (in three dimensions) or $2j-3$ (in two dimensions) bars to be rigid. The Maxwell rule was generalized by Laman's (1970) theorem, which solves the problem of generic rigidity in two dimensions (rigidity that depends only on the topology of the system but does not depend on the specific edge lengths nor joint coordinates). The Laman count has been implemented in the 'pebble game' by Jacobs & Thorpe (1995, 1996). This numerical algorithm can determine the rigidity of an arbitrary generic pin-jointed structure and enumerate its rigid and underconstrained regions. Unfortunately, the pebble game cannot be applied to zeolite frameworks or to the two-dimensional networks considered here. These systems are nongeneric and exist in symmetrical realizations that can make some constraints redundant, and hence the system is not amenable to simple constraint counting.

To overcome these difficulties, one can use the linear algebra method described by Pellegrino & Calladine (1986). This method calculates the rank of the 'equilibrium' or 'rigidity' matrix and identifies infinitesimal motions in the system. These motions can be either finite (where the system can be continuously deformed without deformations of its rigid units) or infinitesimal (where there is deformation of second or higher order).

The flexibility of infinite repetitive structures is much less known. Guest & Hutchinson (2003) generalized the Pellegrino and Calladine matrix method for infinite repetitive structure. They also proved, based on a linear algebra argument, that locally isostatic infinite repetitive structures always have at least one (in two dimensions) or three (in three dimensions) internal mechanisms. More recently, Hutchinson & Fleck (2006) have classified periodic mechanisms and states of self-stress for the kagome lattice.

In this paper, we extend these studies to a larger number of locally isostatic networks. We show that all the networks studied have finite mechanisms that change the volume of the unit cell.

2. Theoretical background

(*a*) *Matrix analysis and kinetic determinacy of repetitive structures*

Pellegrino & Calladine (1986) used linear algebra methods to analyse the flexibility of pin-jointed structures. They described the equilibrium matrix, $\mathbf{A}$, which relates bar tensions, $\mathbf{t}$, with external forces, $\mathbf{f}$, acting on the joints

$$\mathbf{A}\cdot\mathbf{t}=\mathbf{f}. \tag{2.1}$$

The transpose of the equilibrium matrix, the compatibility matrix, **C**, connects the joint displacements, **d**, with bar elongations, **e**,

$$\mathbf{C} \cdot \mathbf{d} = \mathbf{e}. \tag{2.2}$$

The compatibility matrix is an n by $2j$ matrix, where n is the number of bars and j is the number of joints. The number of mechanisms, or floppy modes, f, is related to the rank of the compatibility/equilibrium matrix r by

$$f = 2j - r. \tag{2.3}$$

For the structures that we are considering, there are, on average, just the right number of constraints so that $n = 2j$, so that, for local isostatic networks of the kind we talk about in this paper, the equilibrium matrix **A** in equation (2.1) is square and n by n. This implies that, if we consider a fixed unit cell, and write down a compatibility matrix, the matrix will also be square and n by n. The unit cell is the basic repetitive unit which contains a fixed number of nodes, edges, etc. and which do not change during a deformation. Thus although the area of the cell does change, the contents do not. This repetitive unit may be just the original cell that defines the undeformed lattice itself, or an integer number of such cells in each of the two directions in the plane. However, if we now also allow the unit cell to deform, in two dimensions we get another three deformation parameters (for instance two orthogonal stretches and a shear), and the 'augmented' compatibility matrix will be n by $n + 3$ (Guest & Hutchinson 2003). This matrix is guaranteed to have at least a three-dimensional nullspace (joint movements/changes in shape of the unit cell that, to first order, do not cause extension of bars/deformation of triangles). This nullspace must contain two rigid-body displacements; but this still leaves an orthogonal one-dimensional space. This space *cannot* be a rigid-body rotation, as such a motion is not allowed by the repetitive displacements demanded by the lattice; thus it must be an 'internal' mechanism. This is a subtle argument that results in at least one internal deformation for each repetitive cell. These are infinitesimal deformations, but the argument can be repeated, as the structure is still repetitive after the deformation is made, and hence leads to finite deformation(s) and pathways that are discussed in §3*f*. Because the network is repetitive, it is infinite in extent and therefore no rotational motion is possible. This is because any such rotation would not be consistent with the repetitive nature of the structure. There are of course still the two macroscopic translational modes of deformation that can be achieved at no cost in energy and so are zero frequency or floppy modes, albeit of a trivial kind. Although the absence of rotations might seem trivial, it in fact leads indirectly to observable consequences. What would have been a rotation mode has been converted into an internal deformation by the imposition of a repetitive structure. This is a mathematically rigorous result, illustrated by the many examples in this paper.

There seems at first sight a contradiction here. On the one hand, we are saying that we have locally isostatic networks, which are therefore rigid, while, on the other hand, we are saying there is at least one internal deformation mode. The difference is that having a repetitive structure makes

the network atypical, thus introducing additional floppy mode(s) or internal deformation(s). If the network were truly generic, then it would have no repetitive unit from a geometrical standpoint, and hence would indeed be rigid.

A similar argument applies in three dimensions, where allowing the unit cell to deform gives six deformation parameters, the augmented compatibility matrix is n by $n+6$ and the nullspace must be at least six-dimensional, three of which are simple translational degrees of freedom, which leaves at least three 'internal' mechanisms or floppy modes. Thus, locally isostatic networks, like zeolites, which are made up of corner-sharing tetrahedra, have at least three internal deformation modes if they are repetitive, because such networks are atypical. This leads to a rich behaviour in a wide variety of silica networks (Hammonds *et al.* 1997, 1998) and in zeolites (Sartbaeva *et al.* 2006). Pathways in these networks are also finite, as infinitesimal deformations can be strung together (as in two dimensions), but have much more complexity, which is one motivation for this paper. Studying pathways in two dimensions is so much more tractable, as well as easy to visualize, than studying pathways in three dimensions.

(*b*) *Ring count*

Next we rederive the simple relation between fractions of rings of different sizes. If we replace each triangle with a vertex, and consider each link between triangles as an edge, any network of corner-sharing triangles can be turned into a three-connected net. In this paper, we use the terms net and network interchangeably to describe an infinite set of vertices connected by edges. Thus three-connected nets (or networks) are those obtained when every vertex is joined to exactly three other vertices by edges. For any infinite two-dimensional net, according to the Euler equation (Coxeter 1961), the sum of the number of vertices V and polygons (rings) P per unit cell is equal to the number of edges, $V+P=E$. If we state that there are N_n polygons with n vertices in each unit cell, then $P=\sum_n N_n$. Further, counting the vertices for every polygon, $\sum_n nN_n$, will count each vertex three times; similarly, counting the vertices for every edge, $2E$, will count each vertex three times, so that

$$3V=2E=\sum_n nN_n. \tag{2.4}$$

Thus, substituting into the Euler equation,

$$6P=6E-6V, \tag{2.5}$$

$$6\sum_n N_n=\sum_n nN_n, \tag{2.6}$$

which means that the average ring size is six for any plane net. Thus, it is impossible to build a network that comprises only small rings (fewer than six) or only large rings. The presence of large rings in a network has to be compensated by small rings.

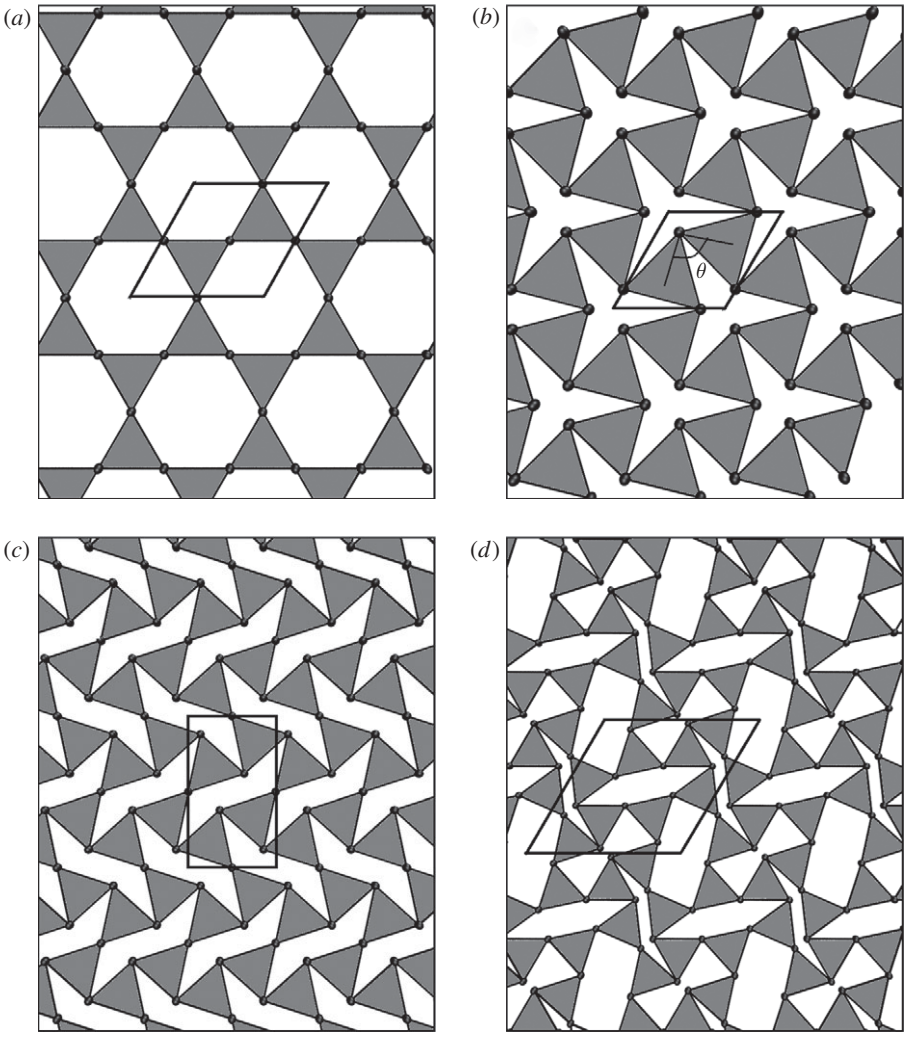

Figure 1. Four different configurations of the kagome topology. (*a*) Minimum density state, with *p*6*mm* plane group symmetry. (*b*) Snapshot of the collapse mode available when there is one hexagon per hexagonal unit cell (*p*31*m* plane group symmetry). (*c*) Snapshot of an alternative collapse mode when there are two hexagons per rectangular unit cell (*p*2*gg* plane group symmetry). (*d*) Snapshot of an additional collapse mode when there are four topologically distinct hexagons per oblique unit cell (*p*2 plane group symmetry).

3. Examples

(*a*) *Kagome lattice*

The simplest network of triangles, the kagome lattice (figure 1), comprises only one type of ring, which according to equation (2.6) must be hexagonal (the corresponding three-connected net is known as the 'honeycomb' net). The infinitesimal collapse mechanisms of the kagome lattice have been studied in detail

by Hutchinson & Fleck (2006). With the smallest unit cell, which has the form of a rhombus with angle $\pi/3$, and consists of only two triangles, the network has only one collapse mechanism, as shown in figure 1*b*. This mechanism reduces the $p6mm$ plane symmetry to $p31m$. For definitions of plane symmetry groups see Hahn (1995). The area of the unit cell is

$$S = a^2 \sin \pi/3 = \sqrt{3} l^2 (1 - \cos \theta), \tag{3.1}$$

where a and l are, respectively, the length of the unit cell and the side of triangle, and θ is an angle between two lines connecting two centres of adjacent triangles. The maximal area, $S_{\max}$, occurs at $\theta = \pi$, and the value of the minimal area, $S_{\min}$, depends on whether triangles are allowed to overlap. If triangles are allowed to overlap ($\theta < \pi/3$), then the unit area vanishes at $\theta = 0$, which means that any finite piece of a kagome lattice collapses into a single triangle, but with a unit cell of zero edge length.

The number of internal mechanisms grows as the relative size of the unit cell increases. Thus, figure 1*c* shows a new mechanism (in addition to the mechanism shown in figure 1*b*) that appears when the unit cell contains two rings. This mechanism adopts plane group symmetry $p2gg$, and can be transformed into the higher symmetry, and vice versa, through the configuration of maximal area (figure 1*a*). The two rings are related by a glide symmetry operation and therefore have equal area, and the new mechanism does not affect the density calculation for the kagome lattice.

A further collapse mode that appears for the 2×2 unit cell is shown in figure 1*d*. Its unit cell has plane group symmetry $p2$, and contains four distinct hexagon configurations. The network maintains a twofold symmetry axis at the middle of each ring. Finally, figure 2 shows one of the collapsing mechanisms in the kagome net with a unit cell that is a 5×5 repeat of the basic kagome cell. The plane group symmetry is $p3$, with nine topologically distinct hexagon configurations.

(*b*) *'Roman mosaic' lattice*

For the next example, we consider the net shown in figure 3, which is made of equal numbers of rhombi and octagons (we will refer to the corresponding three-connected net as the roman mosaic lattice, as it is a tiling pattern found on Roman floors). Some of the collapse mechanisms are shown in figure 3. Since a rhombus has only one internal degree of freedom, defined by the angle θ shown in figure 4, we consider the 'roman mosaic' lattice as tessellations of rhombi. Within the primitive unit cell (four equilateral triangles, delineated by the solid lines) the network has only one mechanism (sheared collapse), shown in figure 3*b*. There is a higher symmetry, face-centred setting $c2mm$ delineated by the dotted cell in figure 3*b*. The area of the oblique primitive cell (shown by the solid lines) is equal to twice the area of the rectangle shown in figure 4. From figure 4, $|AB| = 2l \sin[\theta/2]$ and $|BC| = 2l \sin[\theta/2 + \pi/6]$, thus the area of unit cell, S, is given by

$$S = 2|AB| \cdot |BC| = 4\, l^2 \left[\sqrt{3}/2 - \cos(\theta + \pi/6)\right]. \tag{3.2}$$

The area has a maximum at $\theta = 5\pi/6$ which equals $S_{\max} = 2\, l^2\, (2 + \sqrt{3})$ and a minimum at $\theta = \pi/3$ with $S_{\min} = 2\sqrt{3}\, l^2$.

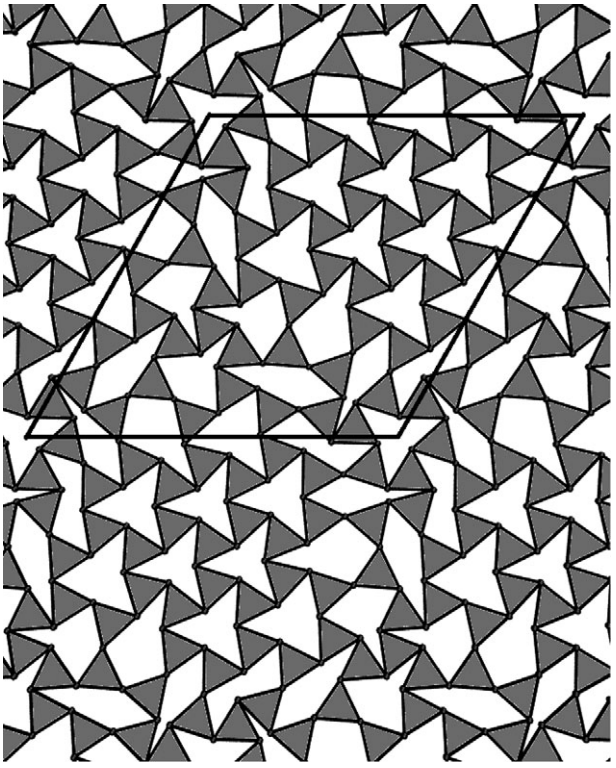

Figure 2. One collapse mechanism of the kagome net with a 5×5 unit cell ($p3$ plane group symmetry).

Two other collapse mechanisms can be found when the unit cell remains square, but now contains eight triangles. The mechanism shown in figure 3*c* (symmetric collapse) can be presented as columns (or rows) of rhombi connected through mirror lines. The unit cell splits into two rectangles with sides equal to $|AB|$ and $|BC|$ and two squares, one with side $|AB|$ and the other with side $|BC|$. Then the unit cell area is

$$S = 2|AB| \cdot |BC| + |AB|^2 + |BC|^2 = 2l^2(2+\sqrt{3})(1-\cos[\theta+\pi/6]). \tag{3.3}$$

The maximal area is $S_{\max} = 4\,l^2(2+\sqrt{3})$ and the minimum area is exactly half this, $S_{\min} = 2\,l^2(2+\sqrt{3})$.

The last mechanism considered here (asymmetric collapse, figure 3*d*) can be viewed as rows of rhombi with two different, alternating sizes. The unit cell area for this case has been solved numerically.

Figure 5 shows the dependency of the area of one unit cell of the Roman mosaic on the angle θ for different collapsing mechanisms. The solid lines correspond to the region where triangles do not overlap ($\theta > \pi/3$). The shear mechanism shows larger changes in unit cell area than the others. Once overlap between triangles is allowed, the structures continue to shrink until the entire infinite net collapses at $\theta = 0$ into a finite structure of a few triangles (similar to the collapse of the

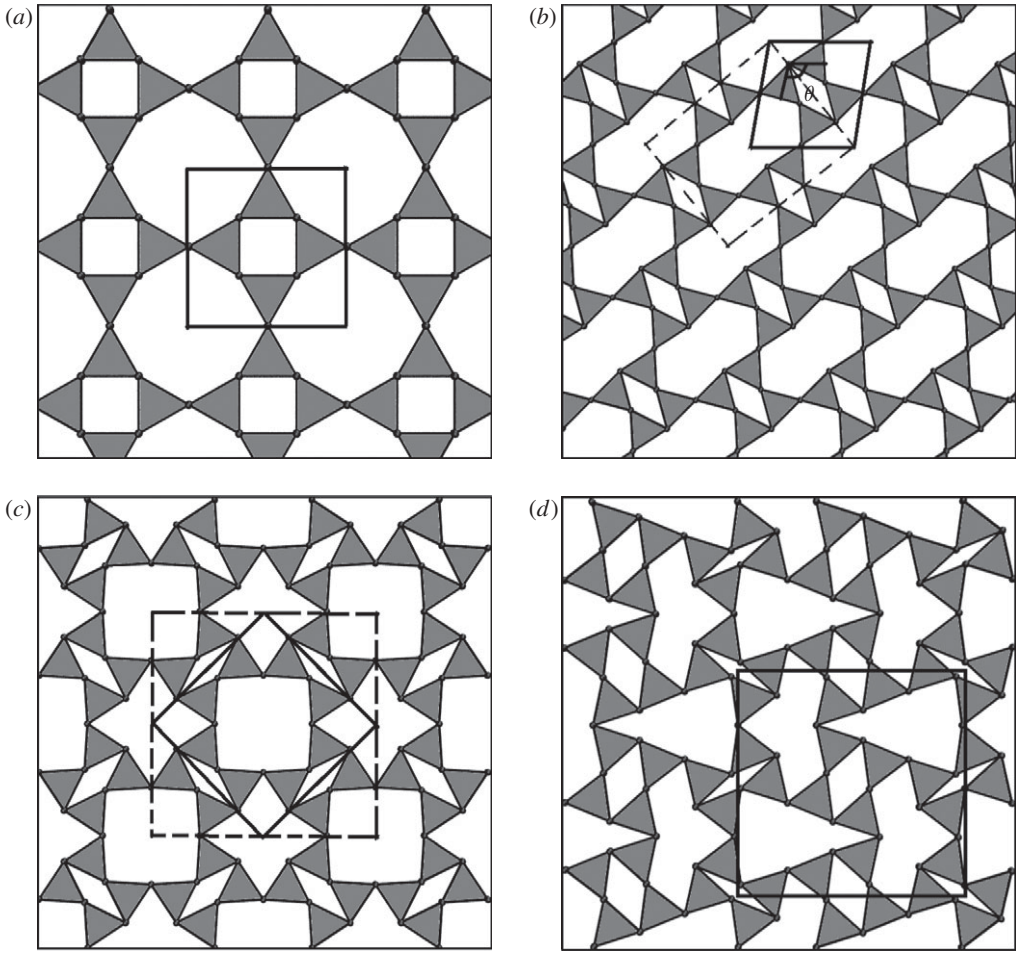

Figure 3. Roman mosaic net. (*a*) Minimum density configuration, *p*4*mm*. (*b*) Snapshot of the shear collapse mode that occurs when there is one octagon and one rhombus per primitive unit cell, *c*2*mm*. (*c*) Snapshot of the high symmetry collapse mode when there are two octagons and two rhombi per square unit cell, *p*4*mm*. (*d*) Snapshot of the low symmetry collapse mode when there are four octagons and four rhombi per square unit cell, *p*2*mg*.

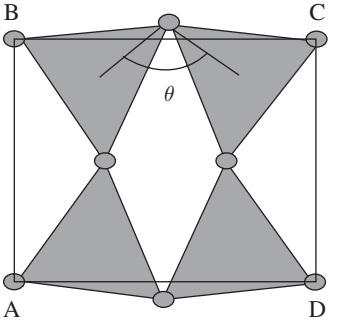

Figure 4. Rhombus area used to calculate the area of the roman mosaic lattice.

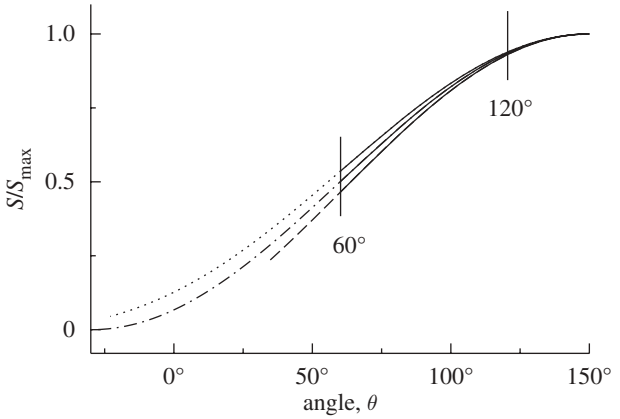

Figure 5. Normalized areas of the Roman mosaic network as a function of the inter-triangle angle in the rhombus. There is a distinct equation of state for each collapse mode. Vertical lines marked 60° and 120° indicate the angles where triangles and oxygens touch (see §3*e* for details; dashed line, sheared mode; dotted-solid line, high symmetry collapse; dotted line, low symmetry collapse).

kagome lattice). The angle θ is zero when the adjoining equilateral triangles lie exactly on top of each other. The dashed line corresponding to the sheared mode stops at $\theta = 34°$. At this point the system flips to the other configuration as shown in figure 6 and continues to collapse to zero area configuration with angle θ fixed at $\pi/3$.

(*c*) *Network with odd rings*

Both the kagome and Roman mosaic networks have even numbers of triangles in each ring, and also have high symmetry, which may increase the number of infinitesimal mechanisms (Guest 2000) by making constraints redundant. Flexibility is not restricted to structures with even rings. The network shown in figure 7 comprises only odd rings (sizes 5 and 7), with a rectangular unit cell of plane group symmetry *pg*, and containing 16 equilateral triangles. Figure 7*a* presents the maximal area configuration, and figure 7*b* demonstrates a collapse mechanism that retains the rectangular symmetry of the unit cell, but alters its aspect ratio.

(*d*) *Large random network*

Our last example, a large random network shown in figure 8, is taken from the computer modelling of vitreous silica (He 1985). This periodic structure was generated by successively introducing 250 defects into an 800-site honeycomb lattice, while maintaining full corner connectivity. The network contains 33.5 per cent pentagons, 24 per cent heptagons and 4.5 per cent octagons and appears disordered. A first-order calculation shows that this network has one infinitesimal collapse mode, and following this path gives an alternative finitely deformed configuration, which is also shown superimposed in the figure.

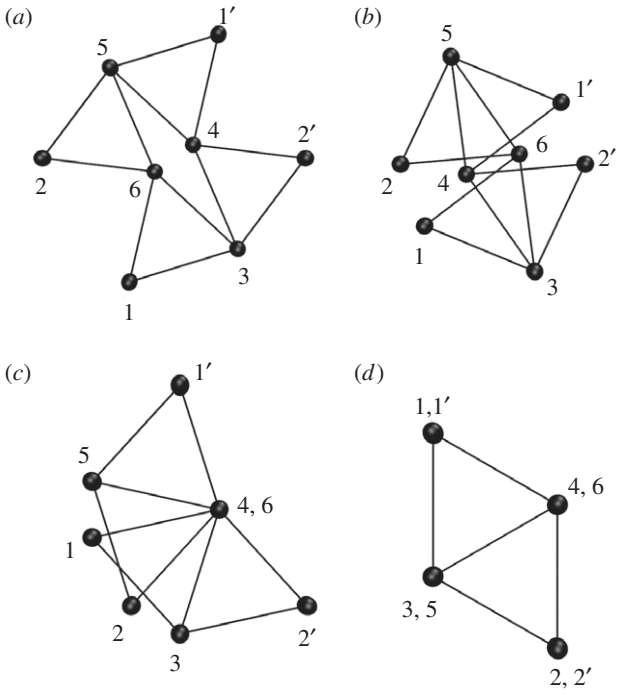

Figure 6. Illustration of the flip associated with the shear mode of Roman mosaic. (*a*) Some large area configuration, (*b*) before flip, (*c*) after flip and (*d*) zero area. Each vertex is labelled with an integer number. Vertices 1′ and 2′ are periodic images of vertices 1 and 2.

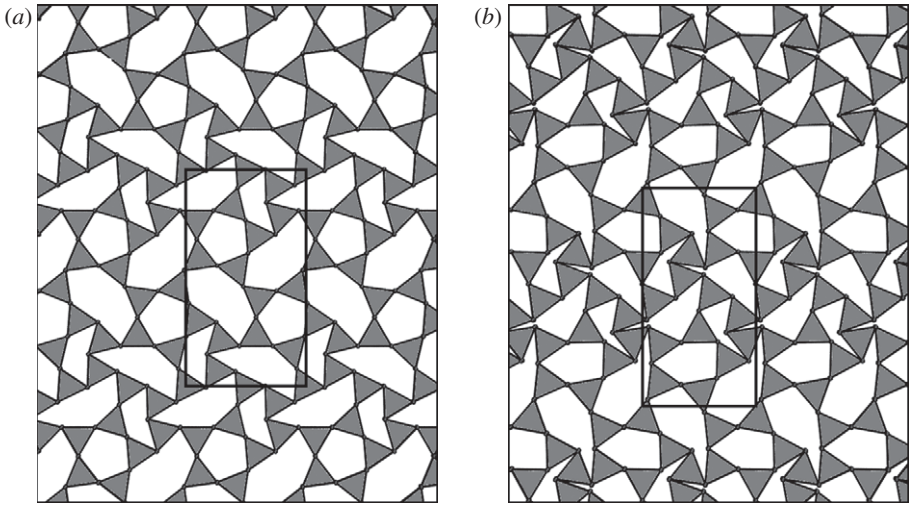

Figure 7. A network with only odd rings, 5-rings and 7-rings in equal numbers. (*a*) Minimum density state (maximum area) and (*b*) an intermediate density state. This net maintains *pg* plane group symmetry during deformation.

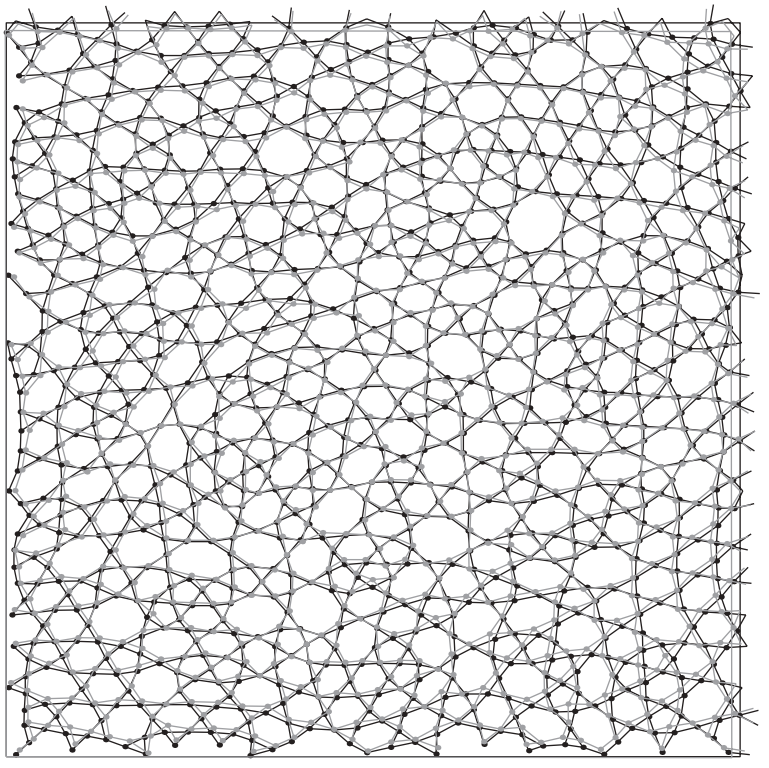

Figure 8. A large random network. Two states are superimposed; the unit cell of the state shown in grey has an area just over 2% smaller than the state shown in black.

(*e*) *Flexibility index*

As a way to measure network flexibility we introduce a flexibility index

$$F = S_{\max}/S_{\min}. \tag{3.4}$$

The maximum area, $S_{\max}$, is defined as the area where triangles are under tension and would start stretching if the area were increased further. We use two different definitions for the the minimum area, $S_{\min}$. In one definition the minimum area occurs when triangles first touch, which corresponds to the density where the smallest angle $\theta_{\min}$ equals $\pi/3$. The other option for the minimum area is related to the definition of the flexibility window in three-dimensional zeolite frameworks (Sartbaeva *et al.* 2006). According to this, each vertex is occupied by an oxygen atom with radius equal to half of the triangle side. Then the minimum area, defined by the touching of oxygen atoms, occurs when the smallest angle equals $\theta_{\min} = 2\pi/3$. Both definitions give rise to flexibility indexes, the former F_Δ and the latter F_{O}, and these are presented in table 1 for different frameworks and their collapse mechanisms. From the definition of the flexibility indices, it is clear that the larger they are, the more flexible the framework is. For rigid structures the flexibility indices equal unity.

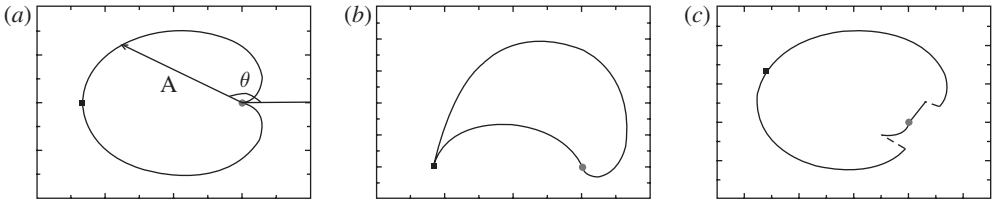

Figure 9. The 'pathway' plot of unit cell area S shown as the length of the radius vs inter-triangle angle θ in polar coordinates. (a) 1×1 kagome net, (b) 2×2 kagome net and (c) shear collapse mode of Roman mosaic net. The solid black square and the solid grey circle represent the maximum and zero areas.

Table 1. Flexibility indices for different collapse mechanisms of various lattices.

lattice	mechanism	F_Δ	F_O
kagome	1×1 (figure 1b)	4	1.333
	2×1 (figure 1c)	4	1.333
	2×2 (figure 1d)	2	1.180
	5×5 (figure 2)	2.187	1.135
roman mosaic	sheared (figure 3b)	2.155	1.077
	symmetric collapse (figure 3c)	2	1.072
	asymmetric collapse (figure 3d)	1.862	1.066
5×7 net	figure 7b	1.553	1.090

(f) *Collapse of networks without repulsion*

In this section we take one further step in our modelling of these two-dimensional isostatic networks, and assume that there is no repulsion between triangles or between vertices. In this purely theoretical situation, compression of the network will continue until the unit cell area becomes zero. In that case, all triangles are lying on top of each other and the entire infinite network becomes a very small system of few (in some cases just one) triangle(s). In the simplest case, the basic collapse mechanism of the kagome lattice shown in figure 1b, the network can be continuously folded from the point of maximum area (figure 1a) to the point of zero area by changing the angle θ from π to 0. At the $\theta = 0$ point, all periodic images of vertices coincide with each other and whole system is reduced to a single triangle. However, there is a second way to collapse the system. It also starts from the maximum area configuration and proceeds by increasing θ from π to 2π. It is easy to see that the final configuration is again just a single triangle, but each intermediate point is the same as in the previous pathway, but related by a symmetry operation. Since the two paths intersect with each other at only two points—maximum and zero areas—they can be combined into one continuous closed pathway, as shown in figure 9a. The pathways shown in figure 9a use the area S as the radius in polar coordinates, and use θ as the usual angle in polar coordinates. For the kagome lattice, the basic collapse pathway has the form of a cardioid given by equation (3.1).

As mentioned earlier, the 1×1 kagome lattice has only one folding–unfolding path. With increasing size of the unit cell, new collapse modes appear. Figure 9*b* represents one such mode in the 2×2 kagome lattice. This pathway has the shape of a highly deformed cardioid. In both the cases mentioned earlier the fundamental unit cells keep their shape ($a = b$, $\gamma = \pi/3$) during compression and at the zero area $a = b = 0$.

It turns out that the collapse pathways of two other systems, the 2×1 kagome (figure 1*c*) and the Roman mosaic net high symmetry collapse, also have form of a cardioid. For the Roman mosaic low-symmetry collapse, it is a deformed cardioid. However, this is not the case for all networks. An interesting example is the shear mode of the Roman mosaic (figure 3*b*). Again, we consider the pathway of the unit cell area S as a function of an intertriangle angle θ. At the maximum area, angle $\theta = 5\pi/6$. Similar to previous cases, there are two collapse paths related to decreasing or increasing θ. At some density, both paths have a discontinuity, shown with dashed lines on figure 9*c*. At that density the system cannot continue to follow the folding path without violation of geometric constraints, so, instead, the system flips to another configuration that has the same density. Both configurations, before and after the flip, are shown in figure 6*b*,*c*. After the flip, the system collapses to zero area, which has a shape of two adjusted triangles (figure 6*d*). During the compression $a = b$, and these go to zero as the area goes to zero. The angle γ decreases from $\pi/2$ to about $2\pi/9$ before the flip and remains fixed at $\pi/3$ after it.

We note that results in this section are often different if a different angle is chosen to display the pathway, and we have found no objective way of selecting which angle to display. Those shown here give particularly 'simple' closed pathways as shown in the three panels of figure 9.

4. Conclusions

We have tested the argument contained in Guest & Hutchinson (2003) about collapsible mechanisms in repetitive, locally isostatic structures. According to this argument, such structures are collapsible with at least one mechanism for plane nets and at least three mechanisms for three-dimensional nets. Our examples are two-dimensional networks of corner-sharing triangles ranging from the kagome lattice, which is the simplest network containing rings of only one size, up to the large random network with 800 triangles. We show that all these structures are flexible. The number of collapse mechanisms grows with the size of the unit cell. But this is still the subject of ongoing work. Results do appear for the number of infinitesimal modes for particular systems, in, for example, Hutchinson & Fleck (2006) and Hammonds *et al.* (1998), but no general rule has been found, nor is there any understanding of how these infinitesimal modes might extend to finite deformations. We have also found that the collapsible mechanisms that preserve the higher symmetry of the network tend to exhibit the widest range of densities without sterical overlap.

This paper was initially developed at the workshop 'Geometric constraints with applications in CAD and biology', organized by Ileana Streinu at Bellairs Research Institute. We acknowledge useful discussions with B. Servatius, H. Servatius and W. Whiteley. We also acknowledge the

financial support of the National Science Foundation grant nos DMR-0703973 and DMS-0714953, and the Donors of the American Chemical Society Petroleum Research Fund for partial support of this research.

References

Coxeter, H. S. M. 1961 *Introduction to geometry.* New York, NY: Wiley.

Earl, D. J. & Deem, M. W. 2006 Toward a database of hypothetical zeolite structures. *Ind. Eng. Chem. Res.* **45**, 5449–5454. (doi:10.1021/ie0510728)

Guest, S. D. 2000 Tensegrities and rotating rings of tetrahedra: a symmetry viewpoint of structural mechanics. *Phil. Trans. R. Soc. Lond. A* **358**, 229–243. (doi:10.1098/rsta.2000.0529)

Guest, S. D. & Hutchinson, J. W. 2003 On the determinacy of repetitive structures. *J. Mech. Phys. Solids* **51**, 383–391. (doi:10.1016/S0022-5096(02)00107-2)

Hahn, T. 1995 *International tables for crystallography*, vol. A. Dordrecht, The Netherlands: Kluwer Academic Publishers.

Hammonds, K. D., Deng, H., Heine, V. & Dove M. T. 1997 How floppy modes give rise to adsorption sites in zeolites. *Phys. Rev. Lett.* **78**, 3701–3704. (doi:10.1103/PhysRevLett.78.3701)

Hammonds, K. D., Heine, V. & Dove M. T. 1998 Rigid-unit modes and the quantitative determination of the flexibility possessed by zeolite frameworks. *J. Phys. Chem. B* **102**, 1759–1767. (doi:10.1021/jp980006z)

He, H. 1985 Computer generated vitreous silica networks and elastic properties of glasses. PhD thesis, Michigan State University, USA.

Hutchinson, R. G. & Fleck, N. A. 2006 The structural performance of the periodic truss. *J. Mech. Phys. Solids* **54**, 756–782. (doi:10.1016/j.jmps.2005.10.008)

Jacobs, D. J. & Thorpe M. F. 1995 Generic rigidity percolation: the pebble game. *Phys. Rev. Lett.* **75**, 4051–4054. (doi:10.1103/PhysRevLett.75.4051)

Jacobs, D. J. & Thorpe M. F. 1996 Generic rigidity percolation in two dimensions. *Phys. Rev. E.* **53**, 3682–3693. (doi:10.1103/PhysRevE.53.3682)

Laman, G. 1970 On graphs and rigidity of plane skeletal structures. *J. Eng. Math.* **4**, 331–340. (doi:10.1007/BF01534980)

Maxwell, J. C. 1864 On the calculation of the equilibrium and stiffness of frames. *Phil. Mag.* **27**, 294–299.

Pellegrino, S. & Calladine, C. R. 1986 Matrix analysis of statically and kinematically indeterminate frameworks. *Int. J. Solids Struct.* **22**, 409–428. (doi:10.1016/0020-7683(86)90014-4)

Sartbaeva, A., Wells, S. A., Treacy, M. M. J. & Thorpe, M. F. 2006 The flexibility window in zeolites. *Nature Mat.* **5**, 962–965. (doi:10.1038/nmat1784)

Treacy, M. M. J., Randall, K. H., Rao, S., Perry, J. A. & Chadi, D. J. 1997 Enumeration of periodic tetrahedral frameworks. *Z. Krist.* **212**, 768–791.

Treacy, M. M. J., Rivin, I., Balkovsky, E., Randall, K. H. & Foster, M. D. 2004 Enumeration of periodic tetrahedral frameworks. II. Polynodal graphs. *Microporous Mesoporous Mater.* **74**, 121–132. (doi:10.1016/j.micromeso.2004.06.013)